Boundary Structures and Changes in Long-Lived Coronal Holes

S. W. Kahler
Air Force Research Laboratory
skahler@solar.stanford.edu

H. S. Hudson
Solar Physics Research Corporation
hudson@isass1.solar.isas.ac.jp

ABSTRACT

Coronal hole (CH) boundaries separate large-scale closed and open solar coronal magnetic fields. We use soft X-ray images from the *Yohkoh* Soft X-ray Telescope (SXT) to investigate the structure and changes of the boundaries of long-lived (several rotations) equatorward-extension CHs which extend from the solar polar regions to midlatitudes. Such extensions appear to move across the photospheric structure, tending to rotate rigidly rather than differentially. Magnetic reconnection must occur at the "closing" boundary in such a case, to maintain the CH integrity. We distinguish three kinds of CH boundaries in the soft X-ray observations. The longest of these lie in large-scale magnetic field regions; these boundaries are generally ragged and not sharply defined. Changes at such CH boundaries appear to proceed gradually, with clear loop brightenings or dimmings only occasionally observed. Boundaries near active regions are sharp and smooth when the adjacent active-region field matches the polarity of the CH field. When adjacent active-region field polarities oppose the CH field polarities, the CH boundaries are characterized by multiple loops connecting the active region fields with fields near the CH. Neither large-scale transient X-ray events nor coronal bright points appeared significant factors in long-term CH boundary development. The large-scale loops at CH boundaries may have long lengths (20° to 30°), but invariably terminate in the quiet corona rather than in another CH boundary. The long loop lengths at some CH boundaries, their gradual motions and brightness changes, and the observation of smooth, straight long-lived boundaries at high latitudes suggest that reconnection of some boundary field lines may occur in the high corona. We consider the cases for reconnection at CH boundaries between open field lines only and between open and closed fields. The role of driven reconnection in low altitude fields in maintaining the CH boundaries is also considered.

Subject headings: Sun: magnetic fields — Sun: corona

1. Introduction

Solar coronal holes (CHs) are large regions of the corona which are magnetically open to interplanetary space (Wang, Hawley & Sheeley 1996). In X-ray images of the Sun they can be seen as dark voids in unipolar magnetic regions, in contrast to X-ray from the surrounding regions of closed magnetic fields (Zirker 1977). Coronal holes are also observed from the ground as reduced absorption regions in the He 10830 Å line (Zirker 1977, Harvey & Sheeley 1979).

At the minimum of the solar activity cycle the Sun is dominated by two polar coronal holes of opposite magnetic polarity. In the mid-latitude regions two kinds of CHs may be observed. The *isolated CHs* are often located near active regions (Wang et al. 1996) and have an occurrence rate that follows the solar activity cycle (Insley et al.

1995). The second kind of CH is the *equatorward extension* of a polar coronal hole. Equatorward extensions were prominent during the *Skylab* mission, which occurred in the declining phase of the solar cycle, but their occurrence rate is fairly uniform during periods away from solar maximum (Insley et al. 1995). They also tend to rotate nearly rigidly, in contrast to the isolated CHs, which tend to rotate differentially with latitude, although somewhat more rigidly than the photospheric differential rotation rate (Insley et al. 1995).

The quasi-rigid rotation of the equatorial-extension CHs occurs in the presence of the solar differential rotation, which tries to shear the photospheric fields at the bases of the CHs. Wang & Sheeley (1993) used a source surface model at 2.5 $R_\odot$ to calculate the positions of the open field lines in a configuration consisting of an axisymmetric dipole field and a bipolar active region oriented east-west near the equator. They found that the model CHs corotated with the nonaxisymmetric driver flux. The magnetic field of the outer corona rotated quasi-rigidly with time and forced the open fields of the CH to corotate approximately with it to prevent a windup of coronal field lines which would violate the current-free assumption of the model interior to the source surface. In general, the role of the nonaxisymmetric flux driver is played by midlatitude active regions in which the fields of one polarity of the active region link to the fields of the same polarity of the polar hole. Extensions of polar CHs across the equator can form when the leading polarity of an active region in one hemisphere is aligned in longitude with the trailing polarity in the other hemisphere to form a unipolar field region from the pole to the opposite hemisphere.

When a northern-hemisphere positive polarity element, say, of a closed field line enters a CH, "...the flux associated with it becomes open and the connection to the southern-hemisphere element is severed. Since the latter element remains within a closed field region, it must immediately connect to another positive-polarity element. It does so by disrupting a neighboring field-line connection, leaving a nearby negative-polarity element to seek a new partner, and so on. An analogous process occurs when a photospheric flux element crosses from an open into a closed region." (Wang & Sheeley 1993). In both cases there is a wavelike motion of flux elements exchanging partners without a significant change in the coronal field configuration.

A different scenario was proposed by Fisk, Zurbuchen & Schwadron (1999a, b), based on a global model of a tilted magnetic dipole with nonradially expanding field lines anchored in a differentially rotating photosphere. The total open magnetic flux at a source surface must remain constant in that model. Field lines are driven by differential rotation in the open regions of the CHs and by coronal magnetic pressure gradients outside those regions. By undergoing continual episodes of magnetic reconnection with coronal loops at low heliomagnetic latitudes, the field lines progress through the corona back to the opposite CH boundary.

Besides forming the separatrices between large-scale open and closed magnetic fields in the corona, CH boundaries are the crucial regions for theories of the source of the slow solar wind. Perhaps the first idea was that the slow solar wind originates on open field lines within CHs but near the boundaries where the magnetic flux tube expansion is largest (e.g., Wang et al. 1996, Bravo & Stewart 1997, Neugebauer et al. 1998). The appearance of white-light blobs in LASCO observations suggested to Wang et al. (1998) that the slowest and densest solar wind originates in helmet-streamer loops but with a major component still originating from inside CHs near the boundaries. *Ulysses* observations have shown that compared with the fast wind, the parameters of the slow solar wind are highly variable and the composition more biased toward elements of low first ionization potential (FIP) (von Steiger et al. 2000). Wang et al. (1996) interpreted this to mean that some open field lines at CH boundaries, which are the source of slow solar wind, will reconnect with adjacent closed field regions to release coronal material with low FIP material. A similar view (Schwadron et al. 1999) is that all the slow solar wind originates from reconnection of open flux tubes with closed loops within the context of a recent heliospheric magnetic field (Fisk et al. 1999a). While the source region of the slow solar wind remains controversial, it appears that the solution to the problem depends on the physics of the magnetic separatrices at the CH boundaries.

Low-latitude CH boundaries have also been

suggested as important factors in coronal eruptive events. Webb et al. (1978) found that large-scale *Skylab* X-ray transients preferentially occurred near CH boundaries in general and growing low-latitude CHs in particular. Gonzalez et al. (1996) also found that the inferred source regions of coronal mass ejections (CMEs) giving rise to intense geomagnetic storms were regions of adjacent growing low-latitude CHs, active regions, and source-surface current sheets, with the acronym CHARCS. Similarly, Bravo et al. (1998) argued that CMEs were most geoeffective when they were associated with flaring active regions near low-latitude CHs. In a separate study of interplanetary magnetic clouds Bravo et al. (1999) found that the solar source regions of the clouds nearly always lay close to low-latitude CHs. In his study of *Yohkoh* X-ray blowouts (XBOs) Bhatnagar (1996) found that they always erupted from or near the boundaries of CHs. With white-light LASCO coronagraph data at the 1996-1997 solar minimum Lewis & Simnett (2000) found the most active CME region to lie close to the equatorial extension of the northern polar CH. All these authors have suggested that magnetic reconnection between the open fields of the CHs and the adjacent closed fields along the CH boundaries can cause or facilitate some CMEs.

Despite the obvious importance of temporal changes in CH boundaries as a guide to understanding the magnetic reconnection of coronal loops and to determining the source regions of the slow solar wind (Wang et al. 1996, Schwadron et al. 1999), little observational work has been done on the morphology or physics of those changes. Kahler & Moses (1990) studied *Skylab* X-ray images of CH boundaries and found that X-ray bright points (BPs) played an important role in effecting both CH boundary expansions and contractions with size scales of $\sim 2 \times 10^4$ km. Bromage et al. (2000) reported that small-scale changes of the boundary of the "Elephant's Trunk" CH appeared on time scales of a few hours in observations with the Extreme ultraviolet Imaging Telescope (EIT). In those cases sections of the CH appeared to close and re-open. In another examination of the Elephant's Trunk CH, Zhao et al. (1999) found that day-to-day variations in the calculated open field regions only roughly matched the day-to-day variations of the 10830 Å CH boundaries. This suggested that not only the changing photospheric fields but also the interactions between the coronal field and plasma flow are responsible for the changing CH boundaries.

The accumulation of nearly 10 years of solar full-disk X-ray images with good spatial (< 10 arc sec) and temporal (< 1 hr) resolution with the Soft X-ray Telescope (SXT) (Tsuneta et al. 1991) on the *Yohkoh* spacecraft now gives us the opportunity to examine CH boundaries in some detail and to address the recent ideas for coronal magnetic reconnection. The best cases in which to look for evidence of significant reconnection are the low-latitude extensions of polar CHs, which are known to show rigid rotation (Zirker 1977, Wang & Sheeley 1993, Zhao et al. 1999). Their largest divergence from differential flow profiles occurs around or above a latitude of 45°, where the rate of change of the rotation profile is largest (Zhao et al. 1999). We select three CHs from the SXT data for this study. We first describe the magnetic structures at the CH boundaries and briefly compare the X-ray and He 10830 Å observations of CH boundaries. After an examination of the changes in the CH boundaries, we conclude with a discussion of scenarios for the magnetic reconnection process at the boundaries.

2. Data Analysis

We examined the entire data base of SXT observations on laser video disks, looking for good cases of midlatitude extensions of polar holes. Because of the significantly decreased coronal X-ray brightness and more poorly defined CH boundaries around the period of solar minimum in 1996, similar to the 1976 case two cycles earlier (Kahler, Davis & Harvey 1983), we did not consider CHs from that period. This precluded, for example, the Elephant's Trunk extension of the north polar hole of 1996 (Zhao et al. 1999; Bromage et al. 2000). The three cases of this study are listed in Table 1 and identified here as YCH1, YCH2, and YCH3 (YCH for "Yohkoh Coronal Hole"). This nomenclature signifies that we have not made use of other data sets, such as He I 10830 Å, in defining their boundaries. YCH1 was an equatorward extension of the negative polarity south polar hole observed at approximate Carrington lon-

gitudes 90° to 150° over Carrington rotations 1846 to 1849 from September to December 1991. YCH1 is seen prominently in the multilatitude stack plots of Figure 2A of Wang et al. (1996). YCH2 was another equatorward extension of the negative polarity south polar hole, observed at longitudes 40° to 80° over rotations 1851 to 1855 from January to May 1992. YCH3 is a recent equatorial extension of the negative polarity north polar hole, observed longitudes 160° to 190° over rotations 1968 to 1971 from October 2000 to January 2001. Judging from their equatorward extensions, YCH2 and YCH3 rotated at the Carrington period of 27.28 days, but YCH1 rotated with a period of about 26.5 days, moving westward with time.

For each disk rotation of a YCH we selected for observation a 3- or 4-day period of CH passage near central meridian to minimize the projection effects of high coronal loops on the CH boundaries. In general, the divergence of the magnetic fields with height in CHs allows us to determine accurately the locations of CH boundaries when we observe the boundaries within several days of central meridian passage. Image selection was set for one image per hour throughout the day, with typically 15 to 23 images per day resulting for each YCH of Table 1. For some days or disk passages, the data gaps precluded those times from the study, as listed in Table 1. A total of 29 days of SXT observations were used in the analysis, three of which were limited in data coverage to a half day or less. Accounting for data gaps, the total coverage was about 27 days.

Each YCH was examined by making a movie of image sequences using only the long exposures in a single SXT filter. The thin aluminum (Al.1) filter was used for YCH1 and YCH2 in 1991 and 1992, and because of the loss of the SXT prefilter in 1992, the thicker AlMg filter was used for YCH3 in 2000. The movie frame field of view was 256×380 pixels, corresponding to 20.9×31.0 arc min in the usual half-resolution with 2×2 pixels, corresponding to $4.9'' \times 4.9''$. The quarter-resolution (QR) images of 4×4 pixels were resized and combined with the half-resolution images in the movies. For studying the details of the YCH boundaries the half-resolution images were significantly better than the QR images and are used in the figures of this work unless otherwise noted. To track the CH boundaries in time, the initial solar pointing of the movie frame was selectable and the center of the image frame was translated westward through the movie at the rate compensating for solar rotation at the frame center. The brightness table for the images was defined by the standard SXT logarithmic compression to enhance the faint features characteristic of the CH boundaries. Each movie was viewed by stepping through the images as desired. The SXT CH boundaries were compared with those in the daily Kitt Peak National Observatory (KPNO) He 10830 Å synoptic maps and with full-disk magnetograms. We used the magnetograms to determine the general magnetic conditions in and around the CHs but not to do detailed comparisons of SXT features with small (< 0.5 arc min) magnetic features. The goal here was to do a qualitative assessment of CH boundary morphologies, their associations with magnetic field features, and changes in the CH boundaries.

3. Coronal Hole Boundary Structures

A selected SXT image and matching KPNO magnetogram from each of the three recurrent YCHs are shown in Figure 1. The CHs were selected to have boundaries with strong north-south directions, so in the following descriptions we will often differentiate between the basic western and eastern CH boundaries even though the local boundaries may run east-west. While the magnetic fields within CHs are relatively uniform and weak, the appearances and locations of CH boundaries are determined by the fields lying predominantly outside the CHs. In our survey of the CHs we distinguish three basic kinds of boundaries.

3.1. Diffuse Field Boundaries

In terms of total lengths the most prevalent kind of boundary is that located in large scale diffuse coronal fields. We find that these diffuse boundaries at low and midlatitudes are usually ragged, probably reflecting the nonuniformities of the underlying fields, such as the network pattern. Several examples of diffuse CH boundaries are seen in Figure 1. The southwest boundary of the YCH1 runs east to west and lies in a large high-latitude negative field region. The eastern and western boundaries of both YCH2 and YCH3 are also seen in Figure 1 to lie predominantly in large negative field regions. Ragged fields were also character-

TABLE 1
TIMES OF OBSERVATION OF PCH BOUNDARIES.

Yohkoh CH	Longitudes	CR	Dates used	Major data gaps
YCH1, 1991	90°-150°	1847	None	Oct. 4-6
		1848	Oct. 31- Nov. 3	Oct. 31 (6h); Nov. 2 (11h)
		1849	Nov. 25-26	Nov. 27
		1850	Dec. 25	Dec. 25 (9 hr); Dec. 26-27
YCH2, 1992	40°-80°	1851	Jan. 27-29	Jan. 27 (16h)
		1852	Feb. 22-24	
		1853	none	Mar. 20-22
		1854	Apr. 16-19	
		1855	May 13-15	
YCH3, 2000	160°-190°	1968	Oct. 13-15	Oct. 15 (9h)
		1969	Nov. 9-11	
		1970	Dec. 6-8	
		1971	none	Jan. 2-4

istic of the high south latitude east-west boundaries which were prominent features of all three observed rotations of YCH1 and the CR1969 rotation of YCH3.

In several notable cases the diffuse boundaries were smooth. In Figure 2 we show two examples of smooth boundaries extending to at least S50° that persisted throughout a disk rotation. Since in each case we are observing the eastern boundary in the eastern hemisphere, there should be minimal projection effects on the boundaries. This is confirmed by the observation that the locations of the YCH boundaries match those of the KPNO synoptic map of CH boundaries for the corresponding periods. The first example occurred during the CR 1848 rotation of YCH1 and is shown extending southeast from AR6900. The second smooth boundary was observed during the CR 1852 rotation of YCH2, although some ripples developed in the northern end late on February 23, as shown in the bottom panels of Figure 2. Another straight and smooth boundary is seen in the narrow channel in the upper part of the February 22-23 images. These boundaries maintained their integrities along smooth arcs with local deviations of < 10 arc sec; even the ripples observed on February 23 deviated by < 20 arc sec from a smooth arc.

3.2. Matching-Polarity AR Boundaries

The second kind of YCH boundary is that formed near an active region (AR) magnetic field with a polarity matching that of the YCH field. Figure 3 shows examples of AR6901 on 1991 November 1, and AR6982 on 1991 December 25. In these cases, as well as that of the leading negative polarity region of AR9190 on the southeastern boundary of YCH3 in Figure 1, the boundary with the YCH formed by the AR is bright and smooth. We find that as a general rule the YCH boundaries lying near matching-polarity AR fields show this pattern.

3.3. Opposite-Polarity AR Boundaries

The third kind of YCH boundary is that formed near AR fields of polarities opposite that of the YCHs. The right side of Figure 3 shows an example of a complex of ARs with their opposite polarity fields lying along the east-west YCH boundary. Contrary to the second kind of YCH boundary, the opposite-polarity fields are characterized by complexity and multiple loop extensions toward the YCH.

A number of additional examples of opposite-polarity boundaries are found in Figure 1. Both the leading and trailing polarities of AR9190 in YCH3 lie on the YCH boundary, with the leading-

polarity fields forming a smooth same-polarity boundary and the trailing polarity fields forming the complex loop connections to the YCH. In the YCH2 image the leading opposite polarity fields of AR7132 on the southeastern boundary form an arcade of bright loops to connect to the YCH. Another example in the same image is that of the small AR7131 which is $> 20°$ west of the western YCH2 boundary. The opposite-polarity fields of that AR are connected by loops to the western boundary of the YCH. Finally, the 1991 November 1 YCH1 image shows two further examples of AR6900 on the eastern boundary and AR6899 on or near the western boundary. In the latter case the loops are widely divergent from the leading polarity fields into the YCH boundary fields. The opposite-polarity fields of these ARs directly form the YCH boundaries with loops connecting their fields to the weaker fields that border the YCHs. Those loop connections vary considerably, however, depending on whether the nearby YCH boundaries are distant from the AR, as was the case with AR7131 of YCH2; lie on the YCH boundary, as were the cases for AR9190 of YCH3, AR7132 of YCH2, and AR6900 of YCH1; or lie in the YCH, as did AR6899 in YCH1, all shown in Figure 1.

4. Coronal Hole Boundary Activity

The variations of the YCH boundaries are characterized primarily by slow changes with time and size scales undetectable in successive images from the SXT movies. Figure 4 shows two sequences of narrow longitudinal YCH images over one-day intervals with approximate 3-hr cadences. These two days were chosen primarily because of their predominant north-south YCH extensions which allowed us to line up the narrow strips for easy comparison. At the diffuse boundaries little activity is seen either in these sequences or in the movies with approximately hourly cadences that we examined. Some activity occurs in the regions of strong fields, the ARs and small bipoles in particular, but such activity is also generally seen in similar regions far from CHs.

The smooth and fairly straight high-latitude boundaries of Figure 2 provide another example of the lack of activity at diffuse boundaries. In a typical day no discrete events or changes were observed at these boundaries. Both boundaries made angles of about 50° to the meridian and appeared to be undergoing the strong shearing expected from differential rotation. However, we measured the corresponding angles along the same boundaries during the preceding and following rotations, and in each case the angles were the same to within 5° on the preceding rotations (CRs 1847 and 1851) and only somewhat more sheared to about 65° on the following rotations (CRs 1849 and 1853). The basic conclusion is that at all latitudes where there are no strong field regions, changes in YCH boundaries were rarely perceptible as brightness variations.

This absence of brightness variations also applies to the predominantly east-west boundaries observed at high latitude, as mentioned in Section 3 and seen in the 1991 November passage of YCH1, shown in Figures 1 and 3, and in the 2000 November image of Figure 3. At those YCH boundaries the faint loop features of the high latitude coronal structures could be seen apparently rotating eastward in our frame of observation, which followed a fixed solar location centered on a low-latitude point. Thus we saw little evidence of interactions between those open and closed field regions, as they appeared to rotate differentially past each other.

In the few cases where we clearly see discrete loop variations at YCH boundaries we can get some insight into the loop lengths and the closed field regions to which the boundary loops are either connecting or disconnecting. In Figure 5 we show three examples of loop variations. The loops which vary in the 2000 January 27 sequence connect the YCH boundary to a region about 30° distant to the east. The loops from the positive polarity fields of the two ARs in the 1992 April 19 period spanned about 15° and underwent a number of brightness changes on that day, but even in those changes it is difficult to determine whether the loops are opening or closing, undergoing reconnection, or simply brightening in place. The connecting loops of the 2000 December 8 period were about 25° to 30° in length. Note that 10° in heliographic coordinates equals about 120 Mm.

The same range of lengths (15° to 30°) for CH boundary loops is seen in Figure 1. In YCH1 the lengths of the obvious loop connections of the two ARs in the south are about 10°. Several loop sys-

tems are evident in YCH2, some apparently extending from near the equator southward, along a filament channel on the eastern boundary, a distance of 30°. Another loop system extends about 15° to 20° from the western boundary to AR7131 in the west. In YCH3 a network of loops can be seen extending at least 20° from AR9191 in the northern hemisphere to the northeast boundary. In the cases where individual or groups of long-lived or transient loops could be discerned around YCH boundaries, we found that they usually extended directly to the boundaries themselves. In no case did the identifiable discrete loop connections extend from the CH boundary to the boundary of another CH.

In the examination of the YCH boundaries we have looked for cases of large-scale (> 10°) eruptive transient events that may have resulted in significant boundary changes (see the discussion of transient coronal holes in Kahler & Hudson 2001). In the 27 days of observations, we noted four cases of AR eruptions and two eruptions outside ARs. In none of the cases did the transient events appear to produce a change in the YCH boundaries lasting more than about 12 hrs. Figure 6 shows the two transients occurring outside ARs. The high-latitude event on 1991 November 3 lay along an east-west NL, in which, as discussed above, the features of the closed fields on the polar sides of the NLs appeared to rotate differentially past the YCHs with no obvious interactions between the two field systems. The second event, on 1992 May 15, occurred along the northern part of YCH2, which was probably obscured by the coronal loops at the YCH2 eastern boundary. A transient coronal hole lay along the YCH2 boundary, as shown in the 11:06 UT image. In both cases the appearances of the YCHs showed no evidence of significant long-term (> 1 day) changes.

The YCH boundary data were examined for any significant role played by coronal bright points (BPs). Very few BPs were observed within or at the boundaries of YCH1 and YCH2, but a number were observed in the YCH3 data. The images of YCH3 of Figure 4 show several BPs both inside the YCH and outside the boundaries, but in no case did we see any evidence of an interaction with larger loop structures. This was also the case with the BPs seen in the YCH3 image of Figure 1. In our survey of the data we found only a single case at 20:21 UT on 2000 November 10 in which a BP in YCH3 at N45° appeared near the western YCH3 boundary and appeared at the base of a high loop which may have been a westward movement of that diffuse boundary. That was a notable exception, however, to the general lack of any interaction that we found between BPs and YCH boundaries.

5. Discussion

5.1. Observed CH Boundary Changes and Structures

Solar-wind studies continue to focus on CH boundaries either as source regions of slow solar wind or as surfaces separating the fast and the slow solar wind flows. If all CH boundaries were physically similar, this might be a reasonable approach, but we find that the magnetic structures seen in X-rays at CH boundaries are of three basic types, each of which could produce significantly different kinds of interaction between the adjacent closed and open magnetic fields. The AR fields probably provide the starkest comparison. When the polarities of the adjacent AR fields match those of the CH, a smooth boundary with a sharp X-ray brightness gradient usually results, suggesting minimal interaction between the closed AR fields and the open CH fields. In these ARs we often see loops brightening or flaring and appearing to rise, but this is also the case for most ARs. On the other hand, the magnetic interactions between CH fields and AR fields of opposite polarity are much more complex. There are usually numerous and dynamic bright X-ray loops tracing connections between the two regions of opposite polarity and forming part of the CH boundaries. The dynamic nature is more evident when the CH boundary runs east-west, as seen in several ARs of Figure 3, in which case the proper motions of the AR fields would be a continuous source of shear for the loop system. The loop connections are clearly undergoing continuous changes as is evident in our SXT movies, but difficult to demonstrate in still images such as Figures 4 and 5. Such action is also evident when ARs lie along north-south neutral lines.

The third kind of CH boundary feature, the diffuse loops, appears to be the most important for solar wind considerations because they comprise

the largest part of the boundary lengths. Their evolution is the least apparent to us in the X-ray range, so we must deduce their development based largely on what they do not do or show, as we explore in the next section. While we are far from any model to discuss how solar wind may arise at or near CH boundaries, we suggest that the scenario may very much depend on which CH boundary structures are relevant for any particular observation.

We find no significant role for either large-scale transients or BPs in the evolution of YCH boundaries. The occurrence of large-scale transients along CH boundaries (Bhatnagar 1996) has suggested the possibility that transients play important roles in CH boundary evolution. Webb et al. (1978) found that when X-ray transients occurred near equatorial (isolated) CHs, those CHs were statistically likely to be increasing in area over long time scales. However, a direct connection between transients and long-term (> 1 day) CH boundary displacements was not established. In our ~27 days of observations of boundaries of equatorward extensions of polar CHs, we found only six transients on those boundaries, of which four were in ARs and two outside ARs, and none of those could be associated with a long-term change in the CH boundaries. This result, however, does not preclude the possibility that CH boundaries could play a significant role in the production of CMEs, as Bhatnagar (1996) and Bravo et al. (1999) have argued.

Kahler & Moses (1990) examined CH boundary changes over a 20-hr cumulative period with *Skylab* X-ray images of CH1 and found boundary changes associated primarily with the appearances and disappearances of BPs. We do not find a role for BPs in the YCH boundary changes, but there are several significant differences between the two studies. First, the basic time resolution of the *Skylab* study was slightly longer (~90 min versus ~60 min) and the total time period examined was much shorter (20 hr versus 27 days) than in our SXT study. Second, the *Skylab* study was based on the 256 s exposures, in which ~ 10 times as many BPs should be visible compared with the standard 4 s exposures used to compile the *Skylab* BP statistics (Golub, Krieger, & Vaiana 1976). Comparisons of numbers of BPs observed with different instruments are also complicated by differing techniques used to identify the BPs (Nakakubo & Hara 2000). More importantly, the number of BPs seen in the SXT YCHs is probably far fewer than in the *Skylab* CHs because the *Skylab* telescope was more sensitive to lower temperatures than is SXT. Direct comparisons of SXT and EIT FeXII images by Handy & Schrijver (2001) and by Zhang, Kundu & White (2001) confirmed that small size-scale emission features seen in the EIT images were not present in SXT images because the EIT FeXII waveband is much more sensitive to low ($\sim 1.2 \times 10^6$ K) temperatures, as was the *Skylab* waveband. Finally, of the 32 discrete changes of *Skylab* CH boundaries, 29 involved BPs and 20 of those changes involved only the dimension of the BP itself. Because of the short duration of their *Skylab* data Kahler & Moses (1990) could not confirm that any of the changes were long term, i.e. extending to at least one day. We conclude that they observed only short-term changes resulting from the appearances and disappearances of the BPs observed at CH boundaries, a possibility they pointed out. If we exclude their CH boundary changes associated with BPs, then their result of only three other observed boundary changes is consistent with the results of this study.

5.2. Magnetic Reconnection at CH Boundaries

A major goal of our study was to determine the dynamics of coronal magnetic field lines at CH boundaries. We chose several examples of long-lived low-latitude extensions of polar CHs with nearly rigid rotation as cases in which significant activity should occur to offset the effects of differential rotation. We do not directly observe the differential rotation of the weak field areas that give rise to the YCHs, but assume that the rotational rates derived for small photospheric magnetic field features (i.e. Komm et al. 1993) are the relevant rates for the photospheric extensions of coronal fields on both sides of the YCH boundaries. Calculations based on differential rotation rates show that even after a single rotation the extrapolated mid and high latitude CH boundaries are displaced several tens of degrees eastward of their observed positions (Wang and Sheeley 1993, Zhao et al. 1999). The problem therefore is to explain how the coronal fields change at CH boundaries to effect a rigid rotation of the CH against the

effects of differential rotation. *Our basic observational result is that, except at ARs, the processes that maintain the rigid boundaries proceed with no clear signatures in the X-ray images.* The closed fields at CH boundaries are also found to extend at least 10° to 20° away from the boundaries, but not to terminate at another CH boundary.

5.2.1. Open-Open Reconnection

In the context of magnetic reconnection the CH open field lines transported to CH boundaries can form newly closed fields to maintain the CH boundary location by reconnecting only with other open fields or with closed fields. In Figure 7 (top) we show a schematic of such an open field line on the eastern (left) boundary of the CH. The bottom panel shows the result of coronal reconnection of that field line with a nearby open field line of the opposite polarity. The newly closed field line produces a shift of the CH boundary to the west (right).

In the postulated inverse process one footpoint of a closed field line is carried into a CH at the western CH boundary. The field line gradually becomes open as the loop top expands high into the corona. This produces not only a newly opened CH field line at the CH boundary, with an accompanying shift of the CH boundary to the west, but also a newly opened field line of opposite polarity in a generally closed coronal region. Since the field lines at CH boundaries diverge significantly from radial, these field line reconnections and openings could occur within coronal streamers, but not necessarily at their boundaries. Reconnection between open fields to produce closed fields and the inverse process of loop conversion to open fields, as considered here, results in changes in the amount of coronal open magnetic flux, but would be expected approximately to balance out between the two boundaries of a long-lived CH.

Several recent observations may support the idea of the opening and closing of field lines in coronal streamers. Outflowing blobs, seen forming in streamer stalks at about 3 to 4 $R_\odot$ in the Large Angle and Spectrometric Coronagraph (LASCO) observations by Wang et al. (1998), have been interpreted in terms of magnetic reconnection of open fields (van Aalst et al. 1999, Einaudi et al. 2001) in streamer current sheets or at the tips of closed magnetic loops (Schmidt & Cargill 2000) in streamers. Similarly, the observation of inflows from about 2 to 6 R⊙ in LASCO images was interpreted in terms of magnetic disconnection of open field lines and their subsequent retraction downwards (Wang et al. 1999, Wang et al. 2000, Sheeley et al. 2001). The correlation of the inflow rate with the Sun's nonaxisymmetric open magnetic flux, and with the low ($< 45°$) latitude open magnetic flux in particular, suggested a close relationship of the inflows to the changes in open flux magnetic field lines accompanying the evolution of nonpolar coronal holes (Sheeley et al. 2001).

One basic problem with reconnection between open coronal field lines is that U-shaped field lines must become disconnected from the Sun at the eastern CH boundary and convected outward, as shown in the lower panel of Figure 7. Those fields should in principle be detectable around 1 AU as electron heat-flux dropouts, phenomena which are only rarely encountered in space (Lin & Kahler 1992). Similarly, closed loop structures should be convected outward from the western CH boundary. An electron heat-flux buildup may occur in such closed-field structures, again, a phenomenon not observed in space (Kahler 1994). An additional problem, at least for the interpretation of inflows as reconnection of open field lines, is that the U-shaped outflowing counterparts are rarely observed (Wang et al. 1999, 2000).

A further problem for open-field reconnection is that the properties of the slow solar wind, such as the low-FIP bias and high elemental charge states and compositional variability (von Steiger et al. 2000), are difficult to understand when both the fast and slow wind are supposed to originate from open field line plasmas. In particular, most of the solar wind variability should be observed on the CH boundary where newly opened field lines supply some of the slow solar wind plasma. The variability should also be reduced at the other CH boundary (usually eastern, as in Figure 7) where previously open field lines are closing. In light of these difficulties, the schematic interpretation for CH boundary reconnection shown in Figure 7 is open to question.

5.2.2. Open-Closed Reconnection

The transition of magnetic field lines at CH boundaries has been incorporated into the coronal field models of Wang & Sheeley (1993) and of

Fisk et al. (1999a, b), both of which assume differential rotation. Both also postulate magnetic reconnection between open field lines and closed loops at CH boundaries. As we discussed in Section 1, Wang & Sheeley (1993) suggested that this process takes place as "waves of reconnection" outside the CH, as newly created open field lines reconnect with adjacent closed field lines to produce a new generation of open field lines, which continue the process. These reconnections would occur in the corona (Wang et al. 1996). A problem for this model is that we see no evidence of this wave of reconnection in the form of loop heatings. If each newly opened or closed field line at the CH boundary generated a wave of reconnection, then some significant changes in loop morphology or brightening should always be observed. Since reconnection presumably results in the release of magnetic energy, a wave of reconnection events should also impose a significant energy requirement on the coronal fields.

The scenario for maintaining CH boundaries proposed by Fisk et al. (1999a, b), discussed in Section 1, rests on a model in which the total open magnetic flux at a source surface must remain constant. In Figure 8, based on the cartoon of Figure 4 of Fisk et al. (1999a), we explore the application of their reconnection scenario to CH boundaries. The open field lines are assumed to be transported eastward (leftward) as a result of the rigid rotation of the CH boundaries. At the western boundary, reconnection of the open field line with a closed field loop acts to transport the open field line and the CH boundary eastward. However, on the eastern boundary the closed loop structures are organized such that the open and closed field lines are parallel and not suitable for reconnection. In that case the reconnection of the open field line must occur with more distant (100-300 Mm) closed loops overlying the next neutral line to the east.

The scenario of Figure 8 may have important implications for the solar wind compositional variations. These variations have been interpreted in terms of a model by Schwadron et al. (1999) in which the reconnection of large coronal loops with open field lines allows the loop plasma to escape on newly opened field lines to produce the slow wind. The low-FIP enhancements in the loops are variable and depend on loop size and conditions in the loop. We see from Figure 8 and the results in Section 4 that the closed loops that open to produce the slow solar wind on the western CH boundary could have a range of sizes, while on the eastern boundary perhaps only the largest loops may reconnect with the open field lines. The resulting slow wind flows from the newly-opened loops would then display a compositional asymmetry between the two sides of the transition region between fast and slow wind flows (Zurbuchen et al. 1999).

If the reconnection of open and closed coronal fields occurs at sufficiently great heights, we might expect that either the energy or the resulting rate of energy release would be too small to observe as X-ray loop brightenings in the SXT images, hence explaining our basic observational result. When this basic scenario occurs in streamers, it has the advantage of maintaining the streamer in a quasi-steady state and so may be the preferred alternative interpretation of reconnection for the outflowing streamer blobs (Wang et al. 1998, 2000). Wang et al. (2000) estimated that the flow transit timescale $r/v \sim 10$ hr for a ray or loop to fade or brighten after reconnection. This matches the time scale of $\tau \sim 10$ hr found for the ionization-state abundance variations in the slow wind (Zurbuchen et al. 2000).

5.3. Photospheric Magnetic Fields at CH Boundaries

This study of CH boundaries has been limited to the coronal features observable in the SXT images. We have not dealt with the dynamics of the underlying photospheric fields that anchor the footpoints of the coronal fields at CH boundaries. The basic element for the organization of photospheric fields is the supergranule, which has a timescale of one to two days and a size scale of $\sim$ 30,000 km (e.g., Schrijver et al. 1997). Recent high-resolution observations of quiet photospheric magnetic fields with the Michelson Doppler Imager on *SOHO* have shown a continual random emergence of bipolar fields within supergranules (Schrijver et al. 1997, 1998), with the bipolar footpoints drifting to the network boundaries where reconnection with existing field concentrations occurs. The turnover time, i.e., the time for the magnetic flux emergence to replace completely the flux present at a given time is estimated by Schri-

jver et al. (1998) to be $\sim$ 40 hr. They further estimate that in that time the random walk distance of flux elements is $\sim$ 13,000 km. This distance is comparable to the long-enduring maximum deviation from smoothness of 10 arc sec, equal to $\sim$ 7,000 km, found in Section 3 for the high-latitude YCH boundaries of Figure 2. Thus, we could explain the continued smoothness of the YCH boundaries in the presence of field-line diffusion as resulting from the limited lifetimes of the photospheric footpoints of the boundary loops. In fact, Schrijver et al. (1998) suggest that the rapid flux replacement can act as a 'lubricant' to relax the shear that is built up in the coronal fields by differential rotation. Reconnection is forced to occur through flux replacement to maintain a quasi-potential field configuration and smooth out the irregularities expected from supergranular diffusion.

The magnetic reconnection in CH boundary loops envisioned in this scenario of rapid flux turnover might be expected to occur within $\sim$ 14 to 18 Mm ($\leq 1.5°$) of the photosphere, the maximum observed lengths the EIT FeXII loops associated with emerging flux attain (Handy & Schrijver 2001) before they fade or reconnect. With the YCH boundary loop lengths ranging from $\sim 10°$ to 30°, the reconnection with emerging flux would therefore occur close to the loop footpoints rather than high in the corona, as envisioned in the Fisk et al. (1999a, b) and Wang et al. (1996) models of CH fields. However, the Handy & Schrijver (2001) study applied only to small size scale and cool ($\sim 1.6 \times 10^6$ K) features and excluded the large size scale 'haze', which may well be the CH boundary structures we are considering. The large loops of their study tended to be associated with large concentrations of magnetic flux for which the small size scale flux diffusion may not be relevant. Thus, the magnetic reconnection to maintain the CH boundaries may well occur high in the corona, but the role of the associated photospheric fields is unclear at this time.

6. Conclusions

We find three kinds of X-ray boundaries in the YCHs. The connections between opposite-polarity active-region fields and YCH fields are usually composed of bright dynamic loops. Same-polarity active-region field boundaries are sharp and bright while the most common boundaries, formed by loops tracing large-scale ($> 10°$) coronal fields are generally diffuse and ragged. Changes in the boundaries are nearly always subtle and gradual, suggesting that as the boundaries change through magnetic reconnection, the energy of the reconnection process is too small to produce observable X-ray signatures. There does not appear to be an important role for either BPs or large-scale transient events in maintaining the YCH boundaries.

We have interpreted the gradual changes in CH boundaries in terms of magnetic reconnection in the corona, considering the two fundamental possibilities of reconnection between open and closed fields and between open fields only. The former interactions do not allow for variations in the coronal open flux, although that quantity varies by up to a factor of 2 (Sheeley et al. 2001). The latter would lead to magnetic fields completely detached from the Sun and other fields in the form of closed loops stretched into space, both of which appear to be found rarely in the solar wind. Reconnection between low-lying photospheric magnetic loops and the footpoints of large-scale coronal loops on CH boundaries may play a significant role in facilitating the accommodation of CH boundaries to differential rotation.

A "Window on Asia" grant from the Air Force Office of Scientific Research supported the work of S. K. We thank T. Kosugi for his hospitality during the stay of S. K. at the Institute of Space and Aeronautical Science. H. H.'s work was supported under NASA contract NAS 8-37334. N. V. Nitta provided valuable assistance with the *Yohkoh* software, and we thank N. Schwadron for helpful discussion. NSO/Kitt Peak data used here are produced cooperatively by NSF/NOAO, NASA/GSFC, and NOAA/SEL.

REFERENCES

Bhatnagar, A. 1996, Astrophys. Space Sci., 243, 105

Bravo, S., & Stewart, G. A. 1997, ApJ, 489, 992

Bravo, S., Blanco-Cano, X., & Lopez, C. 1999, J. Geophys. Res., 104, 581

Bravo, S., Cruz-Abeyro, A. L., & Rojas, D. 1998, Ann. Geophysicae, 16, 49

Bromage, B. J. J., Alexander, D., Breen, A., Clegg, J. R., Del Zanna, G., DeForest, C., Dobrzycka, D., Gopalswamy, N., Thompson, B., & Browning, P. K. 2000, Sol. Phys., 193, 181

Einaudi, G., Chibbaro, S., Dahlburg, R. B., & Velli, M. 2001, ApJ, 547, 1167

Fisk, L. A., Zurbuchen, T. H., & Schwadron, N. A. 1999a, ApJ, 521, 868

Fisk, L. A., Zurbuchen, T. H., & Schwadron, N. A. 1999b, Space Sci. Rev., 87, 43

Golub, L., Krieger, A. S., & Vaiana, G. S. 1976, Sol. Phys., 50, 311

Gonzalez, W. D., Tsurutani, B. T., McIntosh, P. S., & Clua de Gonzalez, A. L. 1996, Geophys. Res. Lett., 23, 2577

Handy, B. N., & Schrijver, C. J. 2001, ApJ, 547, 1100

Harvey, J. W., & Sheeley, N. R., Jr. 1979, Space Sci. Rev., 23, 139

Insley, J. E., Moore, V., & Harrison, R. A. 1995, Sol. Phys., 160, 1

Kahler, S. W. 1994, Solar Dynamic Phenomena and Solar Wind Consequences, ESA SP 373, 253

Kahler, S.W., Davis, J.M., & Harvey, J.W. 1983, Sol. Phys., 87, 47

Kahler, S. W., & Hudson, H. S. 2001, J. Geophys. Res., in press

Kahler, S. W., & Moses, D. 1990, ApJ, 362, 72

Komm, R. W., Howard, R. F., & Harvey, J. W. 1993, Sol. Phys., 143, 19

Lewis, D. J., & Simnett, G. M. 2000, Sol. Phys., 191, 185

Lin, R. P., & Kahler, S. W. 1992, J. Geophys. Res., 97, 8203

Nakakubo, K., & Hara, H. 2000, Adv. Space Res., 25(9), 1905

Neugebauer, M., et al. 1998, J. Geophys. Res., 103, 14587

Schrijver, C. J., Title, A. M., van Ballegooijen, A. A., Hagenaar, H. J., & Shine, R. A. 1997, ApJ, 487, 424

Schrijver, C. J., Title, A. M., Harvey, K. L., Sheeley, N. R., Jr., Wang, Y.-M., van den Oord, G. H. J., Shine, R. A., Tarbell, T. D., & Hurlburt, N. E. 1998, Nature, 394, 152

Schwadron, N. A., Fisk, L. A., & Zurbuchen, T. H. 1999, ApJ, 521, 859

Schmidt, J. M., & Cargill, P. J. 2000, J. Geophys. Res., 105, 10455

Sheeley, N. R., Jr., Knudson, T. N., & Wang, Y.-M. 2001, ApJ, 546, L131

Tsuneta, S., Acton, L., Bruner, M., et al. 1991, Sol. Phys., 136, 37

van Aalst, M. K., Martens, P. C. H., & Belien, A. J. C. 1999, ApJ, 511, L25

von Steiger, R., Schwadron, N. A., Fisk, L. A., Geiss, J., Gloeckler, G., Hefti, S., Wilken, B., Wimmer-Schweingruber, R. F., & Zurbuchen, T. H. 2000, J. Geophys. Res., 105, 27217

Wang, Y.-M. 1994, ApJ, 437, L67

Wang, Y.-M., & Sheeley, N. R., Jr. 1993, ApJ, 414, 916

Wang, Y.-M., Hawley, S. H., & Sheeley, N. R., Jr. 1996, Science, 271, 464

Wang, Y.-M., Sheeley, N. R., Jr., Walters, J. H., Brueckner, G. E., Howard, R. A., Michels, D. J., Lamy, P. L., Schwenn, R., & Simnett, G. M. 1998, ApJ, 498, L165

Wang, Y.-M., Sheeley, N.R., Jr., Howard, R.A., St. Cyr, O.C., & Simnett, G.M. 1999, Geophys. Res. Lett., 26, 1203

Wang, Y.-M., Sheeley, N. R., Jr., Socker, D. G., Howard, R. A., & Rich, N. B. 2000, J. Geophys. Res., 105, 25133

Webb, D. F., McIntosh, P. S., Nolte, J. T., & Solodyna, C. V. 1978, Sol. Phys., 58, 389 & Forsyth, R. J. 1997, Geophys. Res. Lett., 24, 2885

Zhang, J., Kundu, M. R., & White, S. A. 2001, Sol. Phys., 198, 347

Zhao, X. P., Hoeksema, J. T., & Scherrer, P. H. 1999, J. Geophys. Res., 104, 9735

Zirker, J., (ed.) 1977, Coronal Holes and High Speed Wind Streams, *Skylab* Workshop I, Colorado Associated University Press

Zurbuchen, T. H., Hefti, S., Fisk, L. A., Gloeckler, G., & von Steiger, R. 1999, Space Sci. Rev., 87, 353

Zurbuchen, T. H., Hefti, S., Fisk, L. A., Gloeckler, G., & Schwadron, N. A. 2000, J. Geophys. Res., 105, 18327

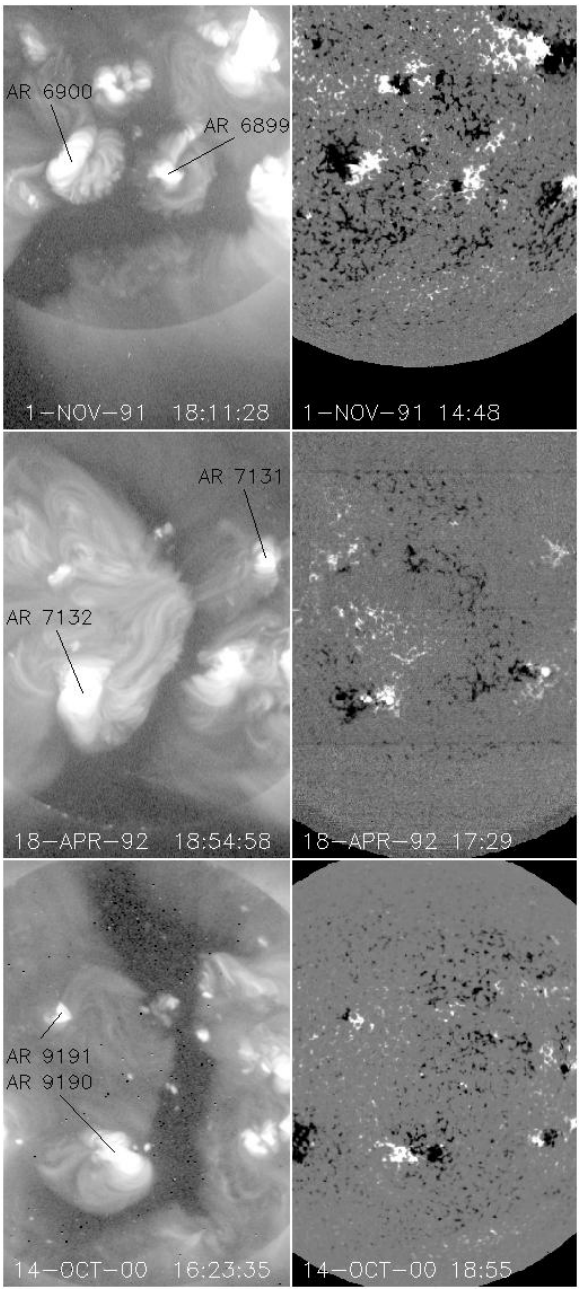

Fig. 1.— SXT images (left) and KPNO magnetograms (right) near selected central meridian transits of the three YCHs of this study. Top: Al.1 image of YCH1 at 18:11 UT on 1991 November 1. Middle: Al.1 image of YCH2 observed at 18:54 UT on 1992 April 18. Bottom: AlMg image of YCH3 observed at 16:23 UT on 2000 October 14.

This 2-column preprint was prepared with the AAS LaTeX macros v5.0.

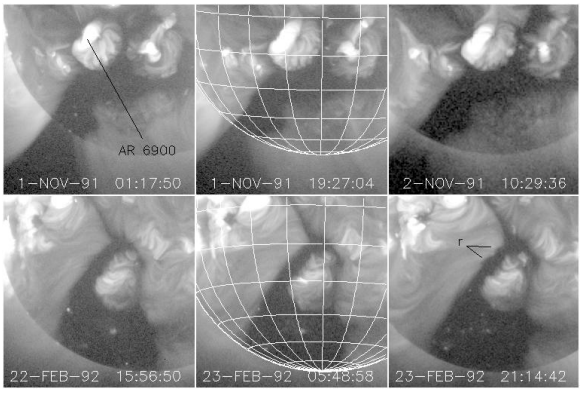

Fig. 2.— Top: Three Al.1 images of the southeast boundary of YCH1 during 1991 November 1-2. The last image is QR. Bottom: Three Al.1 images of the southeast boundary of YCH2 during 1992 February 22-23. Small ripples that developed are indicated by "r". Contrary to the ragged diffuse YCH boundaries evident in Figure 1, these boundaries were very smooth and straight, extending to about S55° in each case. The solar heliographic coordinate grids on this and other figures indicate every 15° of latitude and longitude.

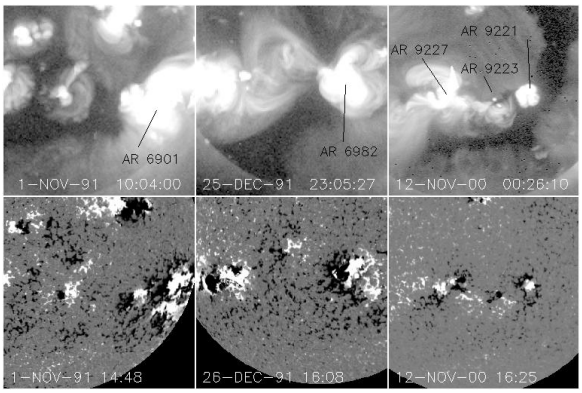

Fig. 3.— Top: Examples of ARs at YCH boundaries. Left: QR Al.1 image of AR6901 on 1991 November 1. Center: Al.1 image of AR6982 on 1991 December 25. The matching polarity fields of these ARs form smooth, curved bright boundaries of the associated YCHs. Right: AlMg image of AR9227, AR9223, and AR9221 running from east to west along the southeast boundary of YCH3 on 2000 November 12. The opposite polarity fields of these ARs form a complex of loop connections to the YCH. Bottom: The associated KPNO magnetograms.

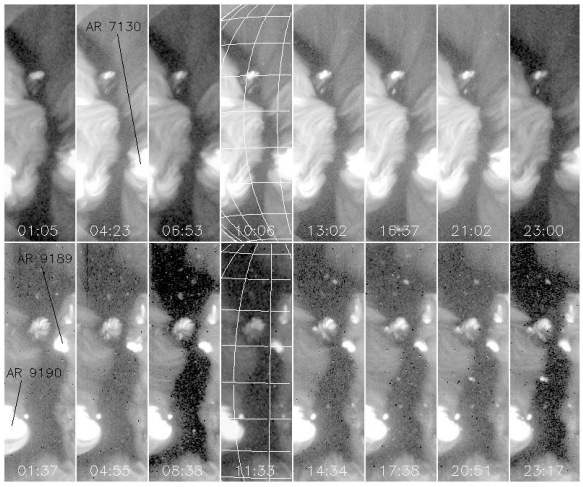

Fig. 4.— Two daily sequences of long north-south YCH passages showing basic slow evolution of the YCH boundaries. In each sequence the frames are centered on a fixed solar longitude, and a solar coordinate grid is placed on one image to indicate locations. Top: A sequence of Al.1 images during the 1992 April 16 passage of YCH2. The 01:05, 06:53, and 23:00 UT images are QR. The principal activity consists of loop motions on the diffuse western boundary near the equator, a brightening of a faint loop eastward of the bipolar region in the northern interior part of the YCH, and loop brightenings and/or motions in AR7130 on the southwestern boundary, all between 13:02 and 21:02 UT. Bottom: A sequence of AlMg images during the the 2000 October 13 passage of YCH3. The 11:33 UT image is QR. At 01:37 UT a small eruptive event occurred in AR9189 on the western boundary, and the bright AR9190 in the southeast showed brightness variations during the day. In the YCH itself small fluctuations occurred in the bipolar region in the north, and two small bipoles emerged east of that region and near the equator at 17:38 UT, but almost no other activity can be discerned.

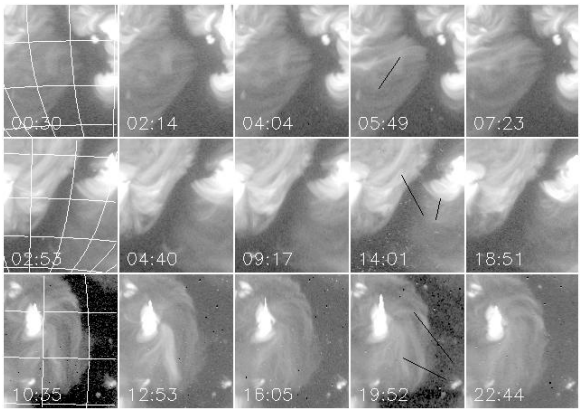

Fig. 5.— Three examples of relatively clear cases of loop variations at YCH boundaries. The solar coordinate grids provide measures of locations and loop lengths. Top: Al.1 images of a sequence of loop activity in a diffuse region of the eastern boundary of YCH2 on 1992 January 27. A shifting of loops, indicated by the black line, is obvious only in the last three panels. Middle: Al.1 images on 1992 April 19 showing subtle brightness changes in loops connecting the western boundary of YCH2 with AR7130 (black line in west) and the eastern boundary with AR7132 (black line in east). Bottom: AlMg images showing activity of loops connecting AR9254 (black line) with the eastern boundary of YCH3 on 2000 December 8.

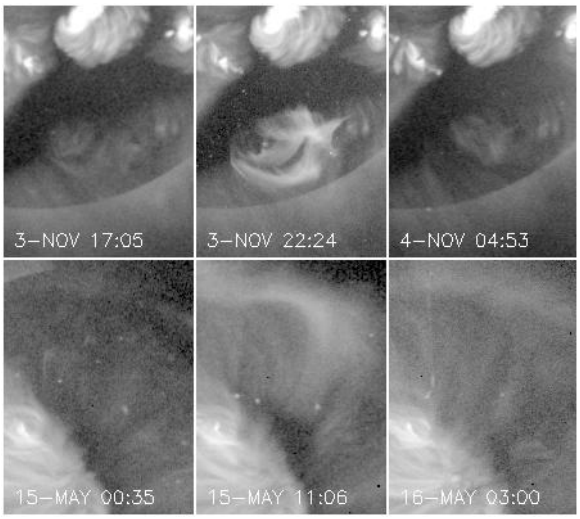

Fig. 6.— Two coronal transients at YCH boundaries. These are the only two cases of transients not involving ARs. Top: Al.1 images of a complex eruption that began about 21:00 UT on 1991 November 3 along an east-west part of YCH1. This event did not appear to produce a long-lasting change on the boundary of that region. Bottom: Al.1 images of a large transient on 1992 May 15 produced an arcade parallel to YCH2.

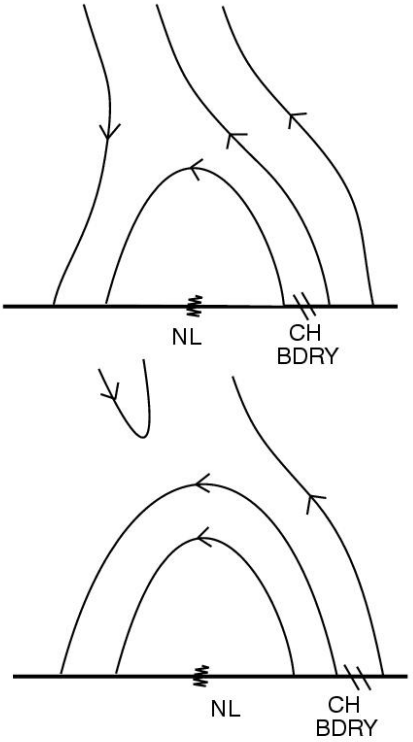

Fig. 7.— Cartoon showing candidate magnetic reconnection scenario at CH boundaries. Top: an open positive field line in a CH is convected to the eastern (left) CH boundary where it meets a closed field loop. Bottom: the open positive field line has reconnected with the open negative field line. This causes the CH boundary to shift to the right. A disconnected U-shaped field line is also released into the upper corona. NL is the magnetic neutral line.

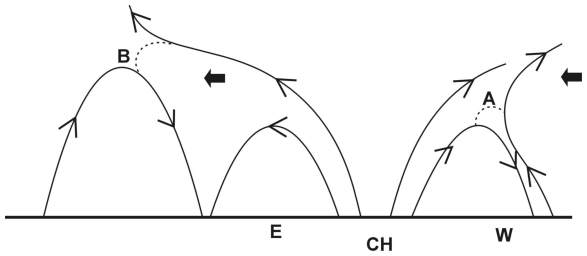

Fig. 8.— Cartoon adapting the model of Fisk et al. (1999a) to show magnetic reconnection at eastern (E) and western (W) boundaries of a rigidly rotating CH. The drift of the magnetic footpoints is assumed to be eastward (thick arrows) relative to the rigid CH boundaries. At the W boundary reconnection takes place (dashed line at A) between the open positive-polarity field line on the right and the adjacent loop to create a new open field line and loop. At the E boundary the open field line cannot reconnect with the adjacent loop because the fields are locally parallel. Instead, the broadly diverging open field line reconnects (dashed line at B) with the more eastwardly distant loop, which presents an antiparallel field to the open field. That reconnection forms a new open field line to the left and a new loop to the right. Both CH boundaries move westward.